



1 Causes of growing middle-upper tropospheric ozone over the 2 Northwest Pacific region

3 Xiaodan Ma^{1,2}, Jianping Huang^{3,4}, Michaela I. Hegglin^{2,5}, Patrick Jöckel⁶, and Tianliang Zhao¹

4 ¹Collaborative Innovation Center on Forecast and Evaluation of Meteorological Disasters, Key Laboratory for
5 Aerosol-Cloud-Precipitation of China Meteorological Administration, Nanjing University of Information Science
6 and Technology, Nanjing 210044, China.

7 ²Institute of Energy and Climate Research – Stratosphere (IEK-7), Forschungszentrum Jülich, Jülich, Germany.

8 ³Lynker, Environmental Modeling Center, NOAA National Centers for Environmental Prediction, College Park,
9 MD, USA.

10 ⁴Center for Spatial Information Science and Systems, College of Science, George Mason University, Fairfax, VA
11 22030, USA.

12 ⁵Department of Meteorology, University of Reading, Reading, United Kingdom

13 ⁶Deutsches Zentrum für Luft- und Raumfahrt (DLR), Institut für Physik der Atmosphäre, Oberpfaffenhofen,
14 Germany

15 *Correspondence to:* Jianping Huang (jianping.huang@noaa.gov)

16 **Abstract.** Long-term ozone (O₃) changes in the middle to upper troposphere are critical to climate radiative forcing
17 and tropospheric O₃ pollution. Yet, these changes remain poorly quantified through observations in East Asia.
18 Concerns also persist regarding the data quality of the ozonesondes available at the World Ozone and Ultraviolet
19 Data Center (WOUDC) for this region. This study aims to address these gaps by analyzing O₃ soundings at four
20 sites along the northwestern Pacific coastal region over the past three decades, and assessing their consistency with
21 an atmospheric chemistry-climate model simulation. Utilizing the European Centre for Medium-Range Weather
22 Forecasts (ECMWF) – Hamburg (ECHAM)/Modular Earth Submodel System (MESSy) Atmospheric Chemistry
23 (EMAC) nudged simulations, it is demonstrated that trends between model and ozonesonde measurements are
24 overall consistent, thereby gaining confidence in the model's ability to simulate ozone trends and confirming the
25 utility of potentially imperfect observational data. A notable increase in O₃ mixing ratio around 0.29-0.82 ppb a⁻¹
26 extending from the middle to upper troposphere is observed in both observations and model simulations between
27 1990 and 2020, primarily during spring and summer. The timing of these O₃ hotspots is delayed when moving
28 from south to north along the measurement sites, transitioning from late spring to summer. Investigation into the
29 drivers of these trends using tagged model tracers reveals that ozone of stratospheric origin (O₃S) dominates the
30 absolute O₃ mixing ratios over the middle-to-upper troposphere in the subtropics, contributing to the observed O₃
31 increases by up to 96% (40%) during winter (summer), whereas ozone of tropospheric origin (O₃T) governs the
32 absolute value throughout the tropical troposphere and contributes generally much more than 60% to the positive
33 O₃ changes, especially during summer and autumn. During winter and spring, a decrease of O₃S is partly
34 counterbalanced by an increase of O₃T in the tropical troposphere. This study highlights that the enhanced
35 downward transport of stratospheric O₃ into the troposphere in the subtropics and a surge of tropospheric source
36 O₃ in the tropics are the two key factors driving the enhancement of O₃ in the middle-upper troposphere along the
37 Northwest Pacific region.

38

39 **Keywords:** EMAC model, ozone sounding, stratospheric intrusion, tropospheric ozone

40



41 **1. Introduction**

42 Stratospheric intrusions and photochemical production are two major contributors to tropospheric ozone (O₃, Ding
43 and Wang, 2006; Neu et al., 2014; Williams et al., 2019; Zhao et al., 2021). The stratosphere accommodates 90%
44 of the total O₃ in the atmosphere. As the largest natural source, downward transport of O₃-enriched air from the
45 stratosphere exerts an important impact particularly on the seasonality of tropospheric O₃ (Williams et al., 2019).
46 Tropospheric O₃ increases of 7% (measured as a partial column between 3-9 km) between 2005 and 2010 over
47 China have been identified as a consequence of increased O₃ precursor emissions and enhanced downward
48 transport from stratospheric O₃ (Verstraeten et al., 2015). While photochemical production is highly dependent on
49 anthropogenic emissions, the impact of stratospheric intrusions on tropospheric O₃ is mainly governed by inter-
50 annual variability and climate-driven changes in the atmospheric circulation (Neu et al., 2014; Albers et al., 2018).
51 Compared to the spatiotemporal variations of O₃ in the lower troposphere, the counterpart in the middle-upper
52 troposphere and their underlying causes remain inadequately quantified, largely due to scarcity of long-term,
53 vertically resolved observational data.

54

55 Chemistry-climate modeling studies demonstrate that climate variability in the atmospheric circulation such as
56 Brewer-Dobson circulation promotes stratospheric intrusions and enhances O₃ abundance in the upper troposphere
57 (Sudo et al., 2003; Young et al., 2018; Akritidis et al., 2019; Griffiths et al., 2020; Liao et al., 2021). A study with
58 a stratospheric chemistry-climate model projects a 20–30% increase in global stratosphere-to-troposphere
59 transport (STT) O₃ flux from 1965 to 2095, as the result of an accelerated stratospheric Brewer-Dobson circulation
60 under an intermediate climate change scenario (Hegglin and Shepherd, 2009). Furthermore, chemistry-climate
61 models (CCMs) predict an even larger increase of the STT O₃ flux (25–80%) under climate change scenarios such
62 as RCP8.5 (Collins, 2003; Sudo et al., 2003; Meul et al., 2018). Notably, Williams et al. (2019) identified an
63 enhanced STT O₃ over Asia and the Pacific region during 1980-2010 based on two different CCMs. Several small-
64 scale processes in proximity to the tropopause lead to irreversible STT events, including Rossby wave breaking,
65 tropospheric cyclones, cut-off lows, and tropopause folding events (Holton et al., 1995). On a regional basis,
66 including East Asia and its coastal area, subtropical westerly jets modulate the location, timing, and frequency of
67 tropopause folds (Sprenger et al., 2003; Albers et al., 2018). Satellite measurements of O₃ and water vapor over
68 six years were used to quantify the impact of a changing stratospheric circulation on tropospheric O₃ in the northern
69 hemisphere (Neu et al., 2014). These observation-based results support the modeling studies that the intensified
70 stratospheric Brewer-Dobson circulation tends to enhance the impact of the stratospheric intrusions on
71 tropospheric O₃. However, the conclusions drawn from the numerical studies have not yet been validated through
72 long-term O₃ measurements, particularly O₃-sounding data (Trickl et al., 2011).

73

74 From 1990 onwards, a significant amount of the anthropogenic emissions responsible for O₃ formation have shifted
75 from North America and Europe to Asia (Granier et al., 2011; Cooper et al., 2014; Zhang et al., 2016). In East
76 Asia, the overall long-term trend of the daytime average near-surface O₃ is 0.45 ppb a⁻¹, contrasting with a trend
77 of -0.28 ppb a⁻¹ in North America in the summertime (April-September) during 2000-2014 (Chang et al., 2017).
78 Several studies have documented the increase in emissions of O₃ precursors at few sites available for evaluating
79 the long-term trends across East Asia (Ma et al., 2016; Sun et al., 2016; Xu et al., 2016; Wang et al., 2017). On
80 the other hand, some regions in East Asia have seen a decline in precursor emissions after 2004, such as Beijing,
81 Hong Kong, and Japan due to local emission control efforts (Krotkov et al., 2016; Liu et al., 2016; Miyazaki et al.,



82 2017; van der A et al., 2017). Elevated NO₂ emissions over megacities in China were possibly transported to Japan,
83 potentially offsetting the local emission control efforts (Duncan et al., 2016). Further research is required to
84 understand the long-term changes in tropospheric O₃, especially in East Asia, where rapid economic growth
85 coincides with strict environmental regulations.

86

87 In this study, we present thirty years of O₃ observations from balloon soundings at fine vertical resolution (less
88 than 10m) with a focus on latitudinal differences. To this end, observations from four sounding sites are analyzed
89 together with model simulation results to quantify the long-term trends of middle-upper tropospheric O₃ and
90 contributions of different origins along the northwestern Pacific coastal region. We are particularly interested in
91 the regional difference near 30°N, the transition zone between the Hadley and Ferrel circulation cells, where the
92 subtropical jet (STJ) prevails and tropopause folding is frequently observed (Škerlak et al., 2015; Zhao et al., 2021).
93 The specific questions to be addressed by this study are 1) How do O₃ trends in the middle-upper troposphere vary
94 with latitude and season over the northwestern Pacific coastal regions and are these observed trends consistent
95 with those derived from a chemistry-climate model? 2) To what extent are these tropospheric O₃ changes linked
96 to stratospheric influences? And 3) to what extent are these tropospheric O₃ changes linked to tropospheric sources,
97 i.e. photochemical ozone production due to biogenic and anthropogenic precursor emissions? The study aims to
98 provide observational evidence to validate and constrain the CCMs' predictions of climate-change impact on
99 tropospheric O₃ in East Asia (e.g., Williams et al., 2019) where such information is still lacking.

100

101 **2. Data and method**

102 **2.1 Ozone-sonde observations**

103 Around thirty years of O₃-sounding data at four sites along the northwestern Pacific coastal regions (Sapporo,
104 Tsukuba, Naha, and Hong Kong) are used to characterize spatiotemporal variations of O₃ in the troposphere.
105 Ozone sondes were launched around 14:00 local standard time (LST) once a week, which corresponds to the time
106 when photochemical production reaches its daily maximum (Oltmans et al., 2004). The ozone-sonde measurements
107 include O₃ partial pressure, temperature, relative humidity, wind speed, and wind direction. Vertical O₃
108 measurements range from the surface to the middle stratosphere approaching 30 km. The Hong Kong site has
109 continually operated the electrochemical concentration cell (ECC) instrument since the beginning of its record.
110 For the three sites in Japan, the O₃-sounding data were measured by Carbon-iodine (CI) ozone sondes with 10-
111 second recording intervals before 2009 and changed to the ECC instrument with 2-second recording intervals. The
112 application of correction factors on ozone profiles during the CI measurement period has been found to
113 inaccurately influence the tropospheric O₃ (Morris et al., 2013). We removed the applied correction factor on the
114 original ozone-sonde data from WOUDC at three Japanese-sounding stations hereinafter. The operating principle
115 of CI ozone sondes and ECC ozone sondes both are based on the reaction of O₃ to potassium iodide solution wherein
116 free iodine is liberated (Johnson et al., 2002; Witte et al., 2018). However, the transition of the measurement
117 technology from CI to ECC around 2009 could lead to an overestimation of uncertainties on the long-term O₃
118 trends. The research from the cross-evaluation of OMI data and the ozone-sonde observation in Japan sites shows
119 that CI ozone-sonde measurements are negatively biased relative to ECC measurements by 2–4 DU compared with
120 the OMI data (Bak et al., 2019). Removing the correction factor in the CI measurements can improve the
121 consistency of ozone sondes with OMI data (Morris et al. 2013). It is worth noting that the conclusion we draw
122 from current available long-term ozone-sonde observation has limitations on the long-term trends but still has



123 important implications on the understanding of tropospheric O₃ changes and model evaluations. The weekly launch
 124 frequency of the ozonesondes has been validated as reliable in representing long-term O₃ trends, as evidenced by
 125 comparing them with near-surface O₃ trends at hourly time resolution (Liao et al., 2021). A summary of
 126 ozonesonde-site location and data availability is presented in Table 1 and Figure 1.

127

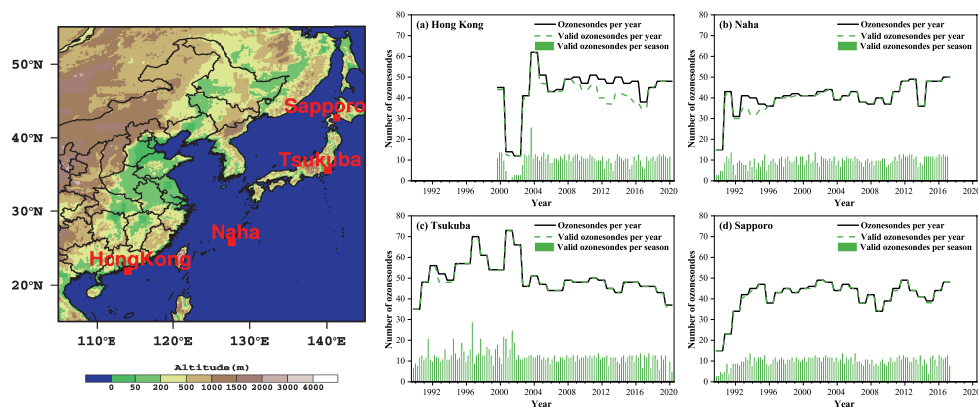
128 We limit our analyses of tropospheric and lower-stratospheric O₃ profiles to altitudes below 18 km and remove
 129 duplicate O₃ values at the same heights in the time series to prevent redundant measurements during the up-and-
 130 down-drops of the floating O₃ sounding balloons. O₃ profiles with continuous data missing more than a 200m vertical
 131 coverage are excluded. The selected valid O₃ profiles with 10s or 2s recording intervals are linearly interpolated
 132 into 10m vertical intervals and then averaged into 50m data points. The O₃ profiles after the quality control with
 133 50m vertical resolution are used for further analysis.

134

135 Due to the latitudinal differences and the seasonal variations in tropopause height across the four O₃-sounding
 136 observation sites, it is inappropriate to apply a specific height as the tropopause height. We thus employ the World
 137 Meteorological Organization lapse rate tropopause definition to calculate the tropopause height (hereafter called
 138 Z_t) for each site and O₃ profile. The Z_t is defined as the level at which the lapse rate decreases to 2 K km⁻¹ or less,
 139 provided that the average lapse rate between this level and all higher levels within 2 km does not exceed 2 K km⁻¹
 140 (WMO, 1957).

141

142 To better compare O₃ levels and trends at different latitudes within the troposphere, we normalize the height of
 143 each O₃ profile into 0~1 by dividing the altitude by the tropopause height Z_t. The upper troposphere (UT) is then
 144 defined by the normalized height (Z/Z_t) range between 0.7 and 0.9. The middle troposphere (MT) and lower
 145 troposphere (LT) are 0.4~0.6 and 0~0.2 Z/Z_t, respectively.



146

147 **Figure 1. Location of O₃-sounding sites and seasonal and annual ozonesonde sampling at a) Hong Kong, (b) Naha, (c)**
 148 **Tsukuba, and (d) Sapporo. The continuous line shows the number of ozonesondes launched per year. The bars show**



149 the corresponding number per season. The dashed line indicates the number of valid ozonesondes reaching up to 18 km
150 altitude.

151 **Table 1. Location of O₃-sounding sites, measurement periods, and total data available along the northwestern Pacific**
152 **coastal region.**

Station	Latitude	Longitude	Elevation (m)	Period	Total data	Valid data (18km)
Sapporo	43.10°N	141.30°E	19	1990-2017	1167	1159(99%)
Tsukuba	36.06°N	140.13°E	31	1990-2020	1564	1556(99%)
Naha	26.20°N	127.70°E	27	1990-2017	1137	1114(98%)
Hong Kong	22.31°N	114.17°E	66	2000-2020	929	863(93%)

153

154 2.2 EMAC model and simulation setup

155 In this study, the European Centre for Medium-Range Weather Forecasts (ECMWF) – Hamburg
156 (ECHAM)/Modular Earth Submodel System (MESSy) Atmospheric Chemistry (EMAC) model is utilized to
157 investigate the long-term changes of tropospheric O₃ and to quantify the relative contributions of different driving
158 factors. The EMAC model is a global model that considers the interaction of chemistry and dynamic processes
159 between the surface and the middle atmosphere (Jöckel et al., 2016). The REF-D1-specific dynamics (SD)
160 simulation results from the EMAC model are used in this study. The REF-D1 experiment is a hindcast simulation
161 of the atmospheric state, using a prescribed sea surface temperature and sea ice from observations along with
162 forcing for the extra-terrestrial solar flux, long-lived greenhouse gasses, and O₃-depleting substances, stratospheric
163 aerosols, and an imposed quasi-biennial oscillation that approximate the observed variations over the historical
164 period to the fullest extent possible (Jöckel, 2023). The hindcast simulations are performed from 1980 to 2019
165 with the SD nudging by Newtonian relaxation towards ECMWF ERA-5 reanalysis meteorological data (Hersbach
166 et al., 2020), including temperature, logarithm of surface pressure, divergence, and vorticity.

167

168 The simulations are conducted at a T42 (triangular) spectral resolution corresponding to an approximately 2.8° ×
169 2.8° quadratic Gaussian grid, 90 hybrid sigma pressure vertical levels from surface up to 0.01 hPa, and with a 720s
170 time step length (Jöckel et al., 2016). EMAC uses chemical submodels, the Module Efficiently Calculating the
171 Chemistry of Atmosphere (MECCA, Sander et al., 2011) and the scavenging submodel (SCAV, Tost et al., 2006)
172 to describe comprehensive chemical reaction mechanisms in gas and liquid phases that include O₃, CH₄, HO_x and
173 NO_x chemistry, non-methane hydrocarbon (NMHC) chemistry up to C₄ and isoprene, halogen (Cl and Br)
174 chemistry, and sulfur chemistry.

175

176 Emissions of lightning NO_x, soil NO_x, and isoprene (C₅H₈) are calculated online for EMAC using the submodels
177 LNO_x (Tost et al., 2007) and ONEMIS (Kerkweg et al., 2006; Jöckel et al., 2016), respectively. EMAC simulates
178 the photolysis (submodel JVAL, Sander et al., 2014) and shortwave radiation schemes (FUBRAD, Kunze et al.,
179 2014) consistently, with particular regard to the evolution of the 11-year solar cycle (Morgenstern et al., 2017).
180 For anthropogenic emissions, mixing ratios of greenhouse gases, ozone-depleting substances (ODS), and other
181 boundary conditions, the EMAC model setup follows the CCMI-2020 protocol of the refD1 hindcast simulations
182 (SPARC, 2021).

183

184 The EMAC model provides the diagnostic tracer O₃S to directly measure the stratosphere-to-troposphere exchange
185 of O₃. The O₃S tracer is transported across the tropopause into the troposphere and is removed by tropospheric O₃



186 reactions (Jöckel et al., 2006; Jöckel et al., 2016). When O₃S re-enters the stratosphere, it is re-initialized (Roelofs
187 and Lelieveld, 1997). The tropospheric O₃ source (O₃T) is here calculated as tropospheric O₃ minus stratospheric
188 O₃ ($O_3T = O_3 - O_3S$).

189

190 To better compare the model results with the observations, the simulation data is extracted from the grid boxes
191 nearest to the observation sites. Specifically, 200 hPa is chosen for Hong Kong and Naha, and 400 hPa for Tsukuba
192 and Sapporo to represent the upper troposphere. The middle troposphere is defined at 500hPa, while the lower
193 troposphere is represented by 850 hPa in the model results. To assess the statistical significance of the differences,
194 a paired two-sided t-test ($p < 0.05$) is conducted for comparison.

195

196 **3. Results**

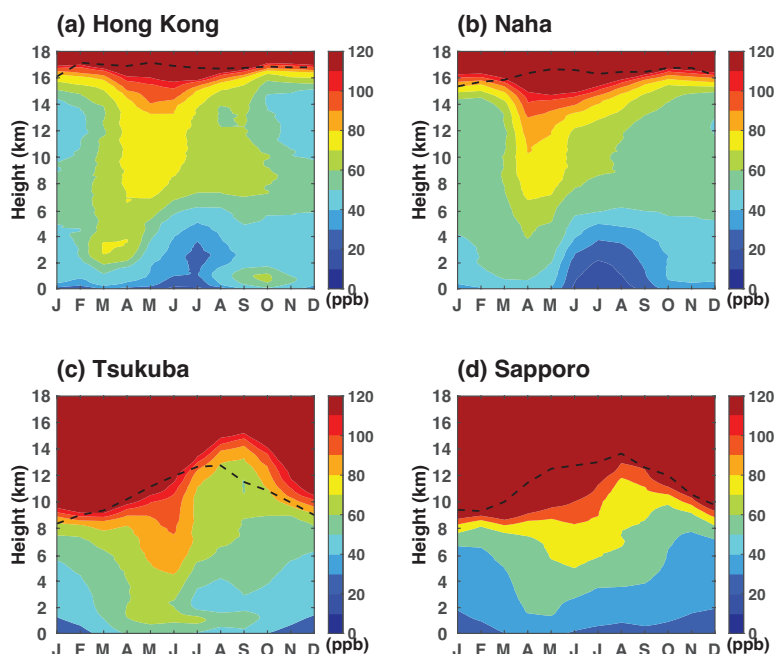
197 **3.1 Observational changes at different stations**

198 **3.1.1 Climatological distribution of tropospheric ozone**

199 Figure 2 depicts the climatologically vertically resolved tropospheric O₃ distribution with respect to months. The
200 four sites all show a distinct tongue-shaped pattern in top-down direction characterized by high concentrations of
201 O₃ greater than 70 ppb, each exhibiting peak levels in distinct months. The ozone tongue extends from the lower
202 stratosphere to the middle troposphere, even further spreading downward to the lower troposphere. In subtropical
203 regions such as Hong Kong and Naha, the ozone tongue starts to appear in early spring. Their appearance becomes
204 progressively delayed when moving towards higher latitudes, with peak occurrences observed in Tsukuba during
205 June and Sapporo in July (Figure 2c-d). For the mid-latitudes over the Pacific region, the incidence of stratospheric
206 intrusions has been found to have a strong correlation with the location of the STJ (Zhao et al., 2021). The
207 northward shift of the STJ with seasons agrees well with the occurrence of ozone tongue in different months over
208 the four sites along the northwest Pacific coastal regions (Figure S2). The tropopause folding on the south part of
209 the STJ could lead to more stratospheric intrusion contributions to the ozone tongue. This suggests a potential
210 contribution of stratospheric intrusion to the seasonal lag of the ozone tongue.

211

212 On the other hand, the four sites display distinct month-height cross-section distribution patterns of O₃. In near-
213 tropical regions such as Hong Kong and Naha during the summer, a relatively "clean" layer with O₃ mixing ratios
214 less than 40 ppbv extends from the surface to about 5.0 km above the ground level (AGL). Such a structure,
215 characterized by low concentrations in the lower troposphere is not observed at the other two high-latitude sites.
216 The unfavorable meteorological conditions linked to the East Asian monsoon like a strong wind, precipitation, and
217 less radiation could lead to significant ozone scavenging and less photochemical production. This suggests that
218 the East Asian summer monsoon has a more significant impact on O₃ vertical structures at lower latitude sites
219 compared to high latitude sites. Meanwhile, it is noticed that high O₃ mixing ratios appear within the atmospheric
220 boundary layer (ABL) (0.7-1.6km according to Su et al., (2017)) in Hong Kong in autumn (Figure 2a), which
221 represents the combined effect of local emissions and regional transport. During this season, the prevailing winds
222 are predominantly from northwest to north, which could bring elevated levels of O₃ and its precursors from the
223 Pearl River Delta region, a major manufacturing base in China, to Hong Kong (Ding et al., 2013; Lin et al., 2021).



224

225 **Figure 2. Month-height cross sections of monthly mean O₃ at four O₃-sounding sites, (a) Hong Kong, (b) Naha, (c)**
 226 **Tsukuba, and (d) Sapporo, from 1990 to 2020 (2000 to 2020 for Hong Kong). Black dash lines indicate the multi-year**
 227 **average tropopause height.**

228

229 3.1.2 Long-term trends in different layers of the troposphere

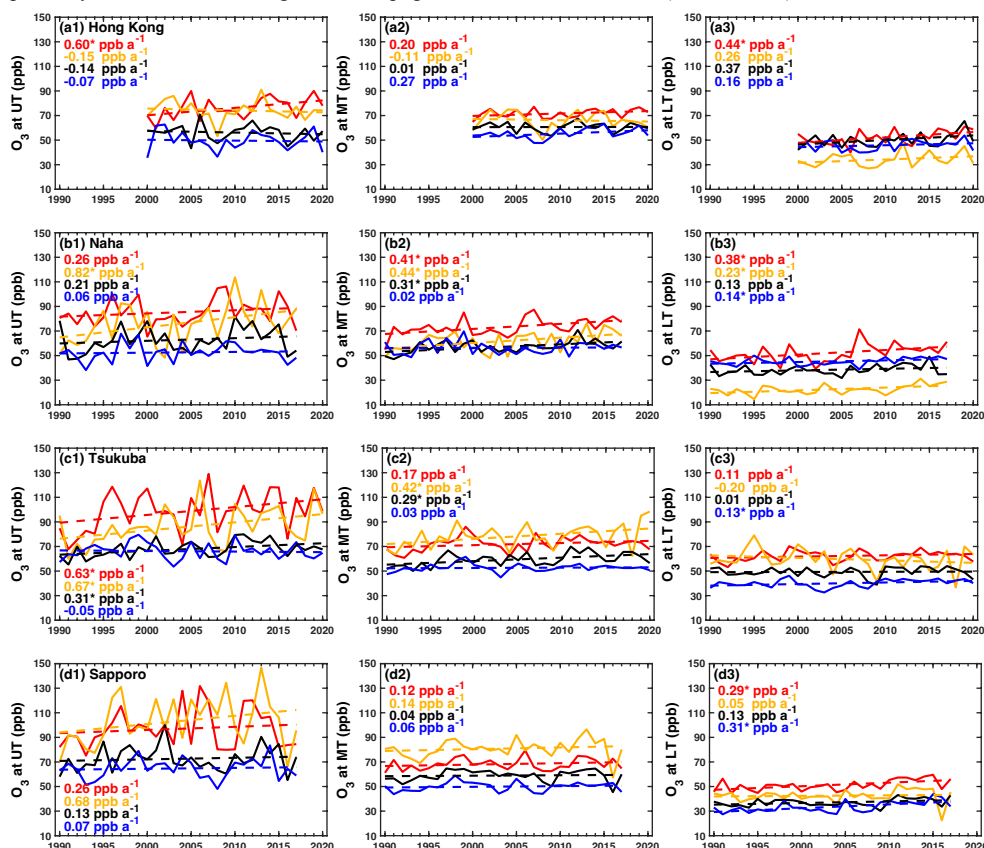
230 Figure 3 presents the long-term trends of O₃ in the upper, middle, and lower troposphere. In general, O₃ in the
 231 upper troposphere shows larger increases during boreal spring and summer than autumn and winter among the
 232 four sites except for Hong Kong. The largest O₃ trends are observed at Naha with an increase of 0.82 ppb a⁻¹ during
 233 the summer and at Tsukuba (0.63 ppb a⁻¹) during the spring (at a 95% confidence level). Hong Kong only shows
 234 a significant O₃ increase in spring with 0.60 ppb a⁻¹ while Tsukuba exhibits extensive O₃ increase except winter.
 235 For the Sapporo site, substantial positive O₃ changes are observed during summer but not statistically significant
 236 due to large temporal variabilities. This finding implies the importance of STJ in the change of O₃ in the upper
 237 troposphere at Naha and Tsukuba. The locations are situated within the transitional zone between the Hadley and
 238 Ferrel circulation cells in spring and summer, as illustrated in Figure S2. This influence appears more pronounced
 239 in comparison to the other two sites, namely Hong Kong and Sapporo, which are situated further from this
 240 transitional zone.

241

242 Moving to the middle troposphere, Naha and Tsukuba consistently display an ozone increase during all four
 243 seasons. The changes at these two sites in spring, summer, and autumn are more evident than those at the other
 244 two sites and winter. This suggests a potential strengthened contribution from regional transport and stratospheric
 245 intrusion for these two sites. In addition, lightning-produced NO_x emissions contribute to major events of O₃ in
 246 the middle-upper troposphere over convection active regions (Liu et al., 2002; Zhang et al, 2012). How those
 247 factors contribute to O₃ enhancement remains a question for further investigations.



248 In the lower troposphere, substantial O₃ increases are observed at all sites in spring except Tsukuba. O₃
 249 enhancement in the lower troposphere over Hong Kong during springtime is associated with either equatorial
 250 Northern Hemisphere biomass burning in Africa or Southeast Asian biomass burning (Oltmans et al., 2004). The
 251 Tsukuba site experienced a slight decrease in summer over the past three decades. Such a decrease could be
 252 primarily attributed to the changes in anthropogenic emissions in East Asia (Li et al, 2019).



253 **Figure 3.** Long-term changes of O₃ in the Upper Troposphere (first column), Middle Troposphere (second column), and
 254 Lower Troposphere (third column) in boreal spring (MAM, red lines), summer (JJA, yellow lines), autumn (SON, black
 255 lines), and winter (DJF, blue lines) at Hong Kong (a1-a3), Naha (b1-b3), Tsukuba (c1-c3), and Sapporo (d1-d3). Trends
 256 with a star symbol (*) indicate significance at the 95% confidence level.
 257
 258

259 Overall, the long-term changes in tropospheric O₃ displayed considerable variability, contingent on the
 260 atmospheric layers (i.e., low, middle, and upper) and the geographical latitude of observation sites. Naha, Tsukuba,
 261 and Sapporo exhibited an increase in the middle-upper troposphere. A substantial rise is observed in the upper
 262 troposphere during summer over Naha (0.82 ppb a⁻¹) and spring over Tsukuba (0.63 ppb a⁻¹). When compared to
 263 the other three sites, changes in the middle-upper troposphere over Hong Kong are smaller or negative, except
 264 during springtime. All four sites demonstrated an increase in O₃ mixing ratios across the four seasons in the lower
 265 troposphere, except for summer in Tsukuba. Investigating the driving factors behind such differences in change
 266 becomes one of the objectives of this study. A more comprehensive exploration of O₃ origin and their contributions



267 to the changes in tropospheric O₃ will be discussed in Section 3.2, leveraging modeling results to provide deeper
268 insight.

269

270 **3.1.3 Changes in composite O₃ cross-sections between decades**

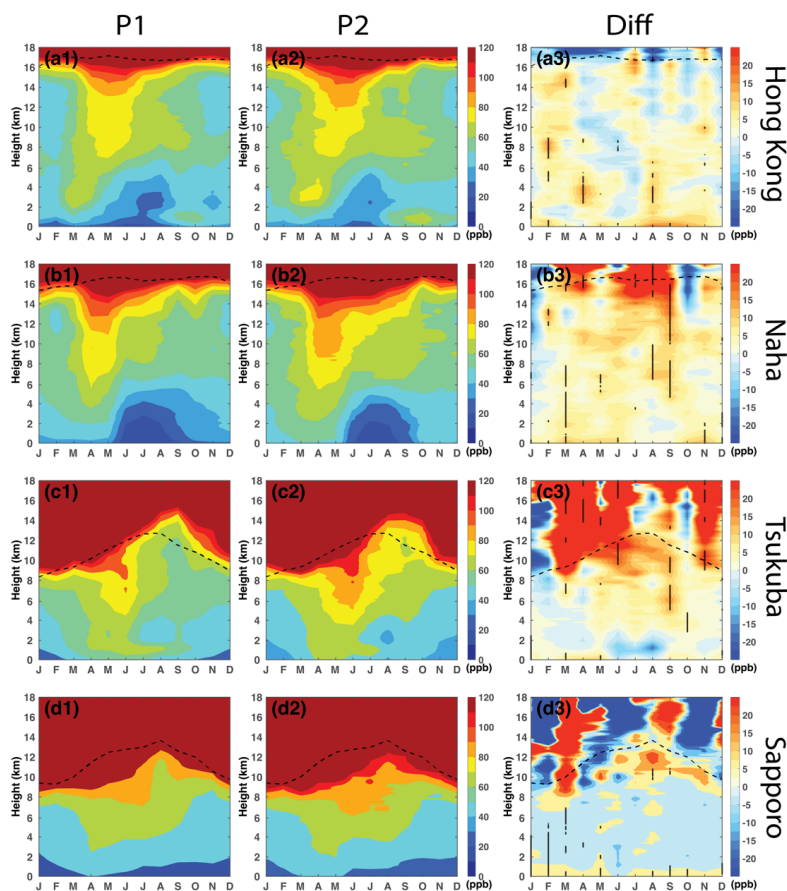
271 Tropospheric O₃ shows a larger variability in the upper troposphere compared to the middle and lower troposphere
272 (Figure 3 a1-d3). Such a large variability, likely driven by transport and dynamics in the tropopause region,
273 impedes drawing definite conclusions on long-term trends for single measurement sites with infrequent sampling.
274 Therefore, the aggregation of tropospheric O₃ during the early and late decades is expected to provide more robust
275 insights.

276

277 Figure 4 illustrates the vertically resolved tropospheric O₃ distributions and changes between the early (the 1990s
278 for Naha, Tsukuba, and Sapporo; the 2000s for Hong Kong) and late (2010s) decades as a function of the month.
279 Their respective tropospheric O₃ changes over the same period (i.e., 2000s to 2010s) at the four sites are presented
280 in Figure S1 to demonstrate the consistency of the results. The time lag pattern for the ozone tongue remains the
281 same from April in the southern site of Hong Kong to July in the northern site of Sapporo for the first and the last
282 decades (Figure 4 a1-d1). However, there are noticeable increases in O₃ mixing ratios and a deeper layer extension
283 of the O₃ concentration greater than 80 ppbv from the stratosphere to the troposphere at Naha and Tsukuba over
284 the past several decades (Figure 4 a2-d2).

285

286 As illustrated in Figure 4 a3-d3, Naha, Tsukuba, and Sapporo exhibit significant enhancements of O₃ from the
287 middle-upper troposphere to the lowermost stratosphere, ranging from 20 to 40 ppb. In contrast to the three sites
288 in Japan, Hong Kong shows more significant O₃ changes in the lower troposphere. The build-up of lowermost
289 stratospheric (LMS) O₃ happens from the winter to spring, thus the STE flux of O₃ normally reaches its peak
290 during late spring to early summer in the extratropical regions (e.g., Škerlak et al., 2015; Albers et al., 2018). The
291 ozone tongue during the spring and summer is possibly associated with enhanced contribution from stratospheric
292 intrusions. While it may be tempting to conclude that such an O₃ increase primarily originates from the stratosphere
293 due to their proximity, observational data alone cannot provide a definite conclusion. Additionally, different
294 locations among the four sites may introduce further differences in O₃ sources.



295

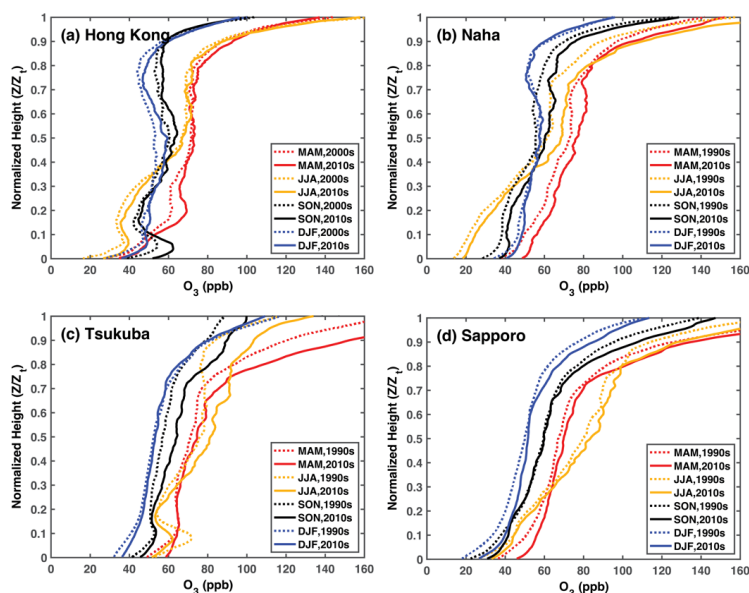
296 **Figure 4.** Month-height cross sections of monthly mean composite O₃ in the first period P1 (1990s for Naha, Tsukuba,
 297 and Sapporo, but 2000s for Hong Kong), the last period (P2: 2010s), and the differences of O₃ between P2 and P1 at
 298 (a1-a3) Hong Kong, (b1-b3) Naha, (c1-c3) Tsukuba and (d1-d3) Sapporo. Black dash lines indicate the tropopause
 299 heights. Dashed lines in the i-l represent the layer with statistically significant changes according to a paired two-sided
 300 t-test ($p < 0.05$).

301

302 Figures 5b-d present a comparison of seasonally-averaged vertical O₃ profiles between the 1990s and the 2010s at
 303 the Naha, Tsukuba, and Sapporo sites. A parallel analysis is conducted for Hong Kong but for a comparison
 304 between the 2000s and 2010s (Figure 5a). While the general trend indicates an increase of O₃ mixing ratios with
 305 altitude, with higher values during spring and summer, several noteworthy features are identified from Figure 5.
 306 Firstly, vertical O₃ profiles vary with latitude and season. For instance, Hong Kong and Tsukuba show O₃ peaks
 307 within the ABL in autumn (black lines) and during summer (yellow lines), respectively. These peaks suggest a
 308 predominant influence of local anthropogenic emissions during the warmer months. A substantial O₃ peak at Hong
 309 Kong is observed around 0.2 normalized height (around 3-4 km above ground level) during spring. This
 310 enhancement is attributed to a combination of stratospheric intrusions and the transboundary transport of biomass-
 311 burning emissions originating from Southeast Asia (Liao et al., 2021; Zhao et al., 2021). On the other hand, Naha



312 and Sapporo do not exhibit discernible peaks in the lower troposphere, suggesting a relatively smaller impact from
 313 the combination of near-surface factors and stratospheric intrusions.
 314
 315 Secondly, the seasonal minimum O_3 mixing ratios in the lower troposphere are observed during summer rather
 316 than winter, contrasting with the middle to upper troposphere observations over Hong Kong and Naha. This
 317 seasonal difference in the lower troposphere could be attributed to the influence of the East Asia Monsoon as
 318 discussed earlier, while not so clear for the seasonal difference in the middle-upper troposphere. Conversely, the
 319 minimum seasonal O_3 mixing ratios occur during winter throughout the entire troposphere at the other two sites.
 320
 321 Thirdly, enhancements of O_3 in the middle and upper troposphere are considerably more pronounced over Naha,
 322 Tsukuba, and Sapporo than over Hong Kong during the warm seasons (spring and summer) over the past three
 323 decades. This enhancement is particularly significant in the upper troposphere in Naha and Tsukuba during
 324 summer, as indicated by the dashed and solid yellow lines. In Hong Kong, enhancements are primarily observed
 325 at the top of the ABL in spring and within the ABL in fall, corresponding to where seasonal maxima are observed.
 326 These findings align with previous research (Huang et al., 2005; Ding et al., 2013; Liao et al., 2021; Lin et al.,
 327 2021).



328
 329 **Figure 5.** A comparison of vertical profiles of seasonal mean O_3 during spring (red), summer (yellow), autumn (black),
 330 and winter (blue) at four sites (a) Hong Kong, (b) Naha, (c) Tsukuba, and (d) Sapporo between the first and the latest
 331 decades.
 332

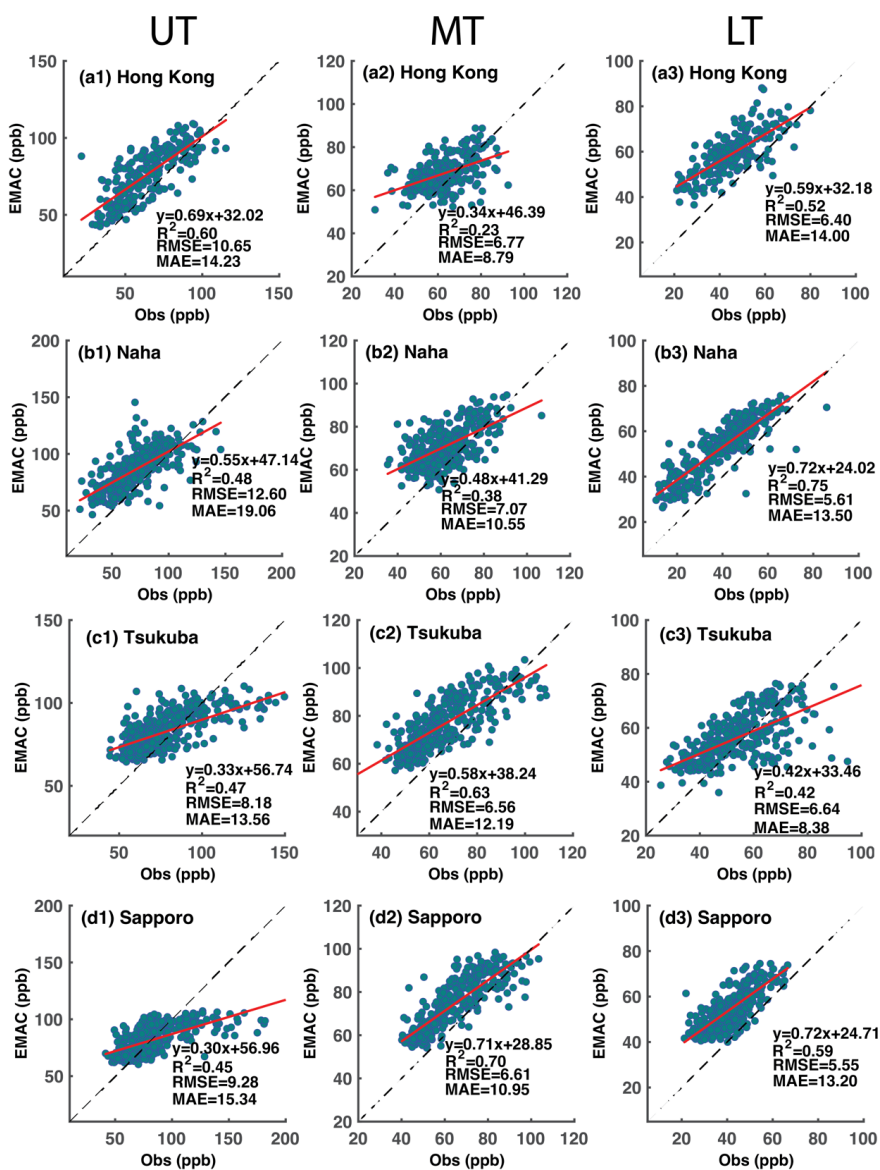
333 3.2 Quantification of stratospheric intrusion versus tropospheric production using EMAC simulations

334 In order to substantiate the observational findings, we now turn to the quantification of the relative contributions
 335 of key drivers to the observed changes in tropospheric O_3 based on the EMAC simulations.
 336

337 3.2.1 Evaluation of EMAC simulations



338 The EMAC simulations of O₃ at different portions of the troposphere are further evaluated with the O₃ sounding
 339 data during the study period. As illustrated in Figure 6, the majority of data points are located above the 1:1 line
 340 at all sites, indicating that the EMAC over-predicts O₃ in the troposphere, which agrees with other related studies
 341 (Jöckel et al., 2016; Young et al., 2018; Revell et al 2018). Meanwhile, the EMAC model shows a better
 342 representation in the upper and lower troposphere than the middle troposphere in Hong Kong and Naha, as
 343 indicated by the coefficient of determinations (R²). For instance, R² reaches to the highest value of 0.75 in the
 344 lower troposphere over Naha (Figure 7c2), whereas R² is only about 0.23 for the middle troposphere over Hong
 345 Kong (Figure 7 b1). As for the mid-latitude sites, Tsukuba and Sapporo, the EMAC model shows a relatively good
 346 representation of O₃ in the different layers of the troposphere, despite the overall overestimation.



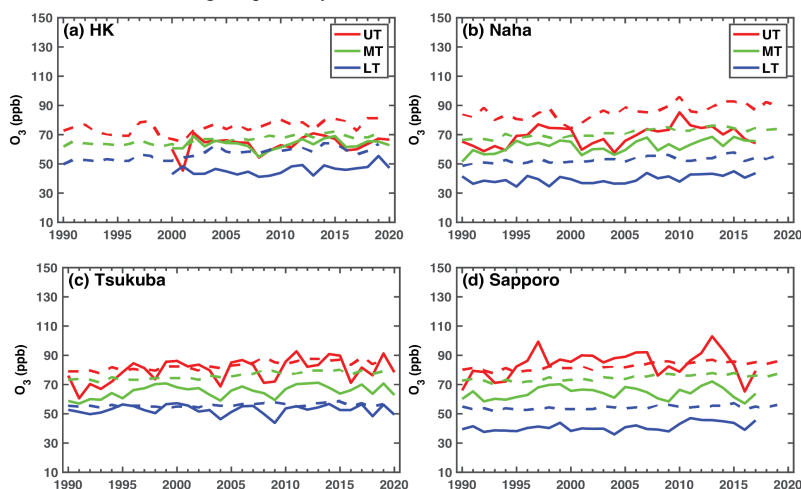
347



348 **Figure 6** Evaluation of O₃ simulated with the EMAC model with observations in the upper troposphere (UT), middle
 349 troposphere (MT), and lower troposphere (LT) at the four sites: (a1-c1) Hong Kong, (a2-c2) Naha, (a3-c3) Tsukuba,
 350 and (a4-c4) Sapporo. The red lines are linear regression results between the observations and the EMAC model results.
 351 Black dash lines are 1:1 for reference. The statistical metrics including the coefficient of determinations (R²), root mean
 352 standard error (RMSE), and mean absolute error (MAE) are included for the quantitative evaluation of the model
 353 performance.

354

355 Furthermore, the EMAC model predicts the realistic long-term trends of O₃ at different levels of the troposphere
 356 as indicated by the similar O₃ changes between observation and model (Figure .7) as well as the comparable long-
 357 term change rates of model-predicted O₃ with the observations (Table 2). For example, the largest positive O₃
 358 trends in the model also occur in the upper troposphere over Naha during summer at 0.75 ppb a⁻¹, slightly less than
 359 the observations with 0.82 ppb a⁻¹ for the past three decades (Table 2). Except for Hong Kong, the other three sites
 360 in the north have larger positive trends of O₃ in the upper troposphere than in the middle and lower troposphere
 361 from spring to autumn. Hong Kong shows a relatively large positive trend of O₃ in the middle and lower
 362 troposphere than other sites during the past 30 years.



363

364 **Figure 7.** Time series of ozone in ozonesonde (solid lines) and EMAC model (dash lines) for four sites at different layers
 365 of the troposphere.

366

367

368

369

370

371 **Table 2.** The trends of EMAC-simulated O₃ (ppb a⁻¹) in the upper, middle, and lower troposphere in different seasons
 372 from 1990 to 2019. The observational ozone trends are indicated in parentheses for comparison for the three Japanese
 373 sites. For the Hong Kong site, the O₃ trends since 2000 for both model (the first value) and observations (the second
 374 value) are in the square bracket. Note that observational periods for three Japanese sites are slightly different from the
 375 model (See Table 1). The trends with symbols (*) indicate the 95% confidence level. **Bold** indicates the agreement with
 376 the observations for significance and the sign of the trend, normal font for the sign of the trend but not for significance,
 377 and *italic* for the opposite sign of the trend.

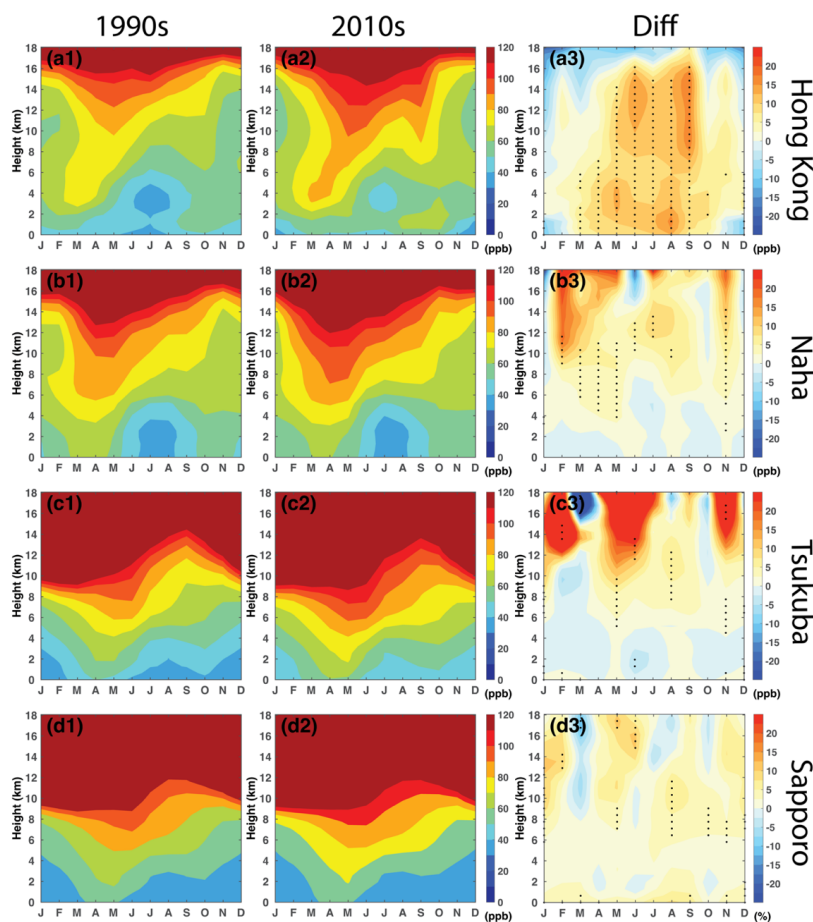


Station		MAM	JJA	SON	DJF
Hong Kong	UT	0.49* [0.98* 0.60*]	0.56* [0.49* -0.15]	0.32* [0.34 -0.14]	0.06 [0.25 -0.07]
	MT	0.33* [0.65* 0.20]	0.43* [0.39* -0.11]	0.36* [0.29 0.01]	0.01 [-0.01 0.27]
	LT	0.49* [0.65* 0.44*]	0.56* [0.53* 0.26]	0.32* [0.16 0.37]	0.06 [-0.18 0.16]
Naha	UT	0.33* (0.26)	0.75* (0.82*)	0.37* (0.21)	0.05 (0.06)
	MT	0.42* (0.41*)	0.33* (0.44*)	0.33* (0.31*)	0.10* (0.02)
	LT	0.32* (0.38*)	0.21* (0.23*)	0.09 (0.13)	0.08* (0.14*)
Tsukuba	UT	0.26* (0.63*)	0.45* (0.67*)	0.32* (0.31*)	0.12 (-0.05)
	MT	0.21* (0.17)	0.37* (0.42*)	0.28* (0.29*)	0.14* (0.03)
	LT	0.13*(0.11)	0.09 (-0.20)	0.03 (0.01)	0.05* (0.13*)
Sapporo	UT	0.22* (0.26)	0.34* (0.68)	0.25* (0.13)	0.15* (0.07)
	MT	0.18* (0.12)	0.28* (0.14)	0.21* (0.04)	0.11* (0.06)
	LT	0.12* (0.29*)	0.12* (0.05)	0.03 (0.13)	0.03 (0.31*)

378

379

380 Figure 8 demonstrates the month-height cross-sections of EMAC-predicted monthly-mean O₃ and their changes
 381 in the troposphere at the four sites between the 1990s and 2010s. Compared with the observed counterparts (Figure
 382 3), the model reproduces the temporal-spatial variation patterns of tropospheric O₃ within the troposphere
 383 quantitatively well. Specifically, the model captures a key feature with the ozone tongue that occurs from late
 384 spring to early summer over four sites and their variation with latitude. The summer relatively "clean" layer with
 385 low O₃ mixing ratios in the lower troposphere at the southern sites of Hong Kong and Naha is also well simulated.



386



387 **Figure 8. EMAC-simulated monthly mean O₃ in the 1990s and 2010s, and their differences between 2010s and 1990s at**
388 **the four observation sites (a1-a3) Hong Kong, (b1-b3) Naha, (c1-c3) Tsukuba and (d1-d3) Sapporo. The horizontal axes**
389 **denote the months of the year and the vertical axes represent the height above ground. Dots in the i-l represent the layer**
390 **with statistically significant changes according to a paired two-sided t-test (p < 0.05).**
391

392 Overall, the EMAC model reasonably simulates the spatial and temporal variations in tropospheric O₃ as compared
393 to the O₃ observations at the four sounding sites. Consistency between the model and observations suggests that
394 the trends observed in the Japanese ozonesondes remain valuable despite uncertainties related to the transitions
395 between the two types of ozonesondes. Moreover, the model can effectively be used to investigate the drivers of
396 these trends.

397

398 3.2.2 Changes in O₃S and O₃T derived from EMAC simulations

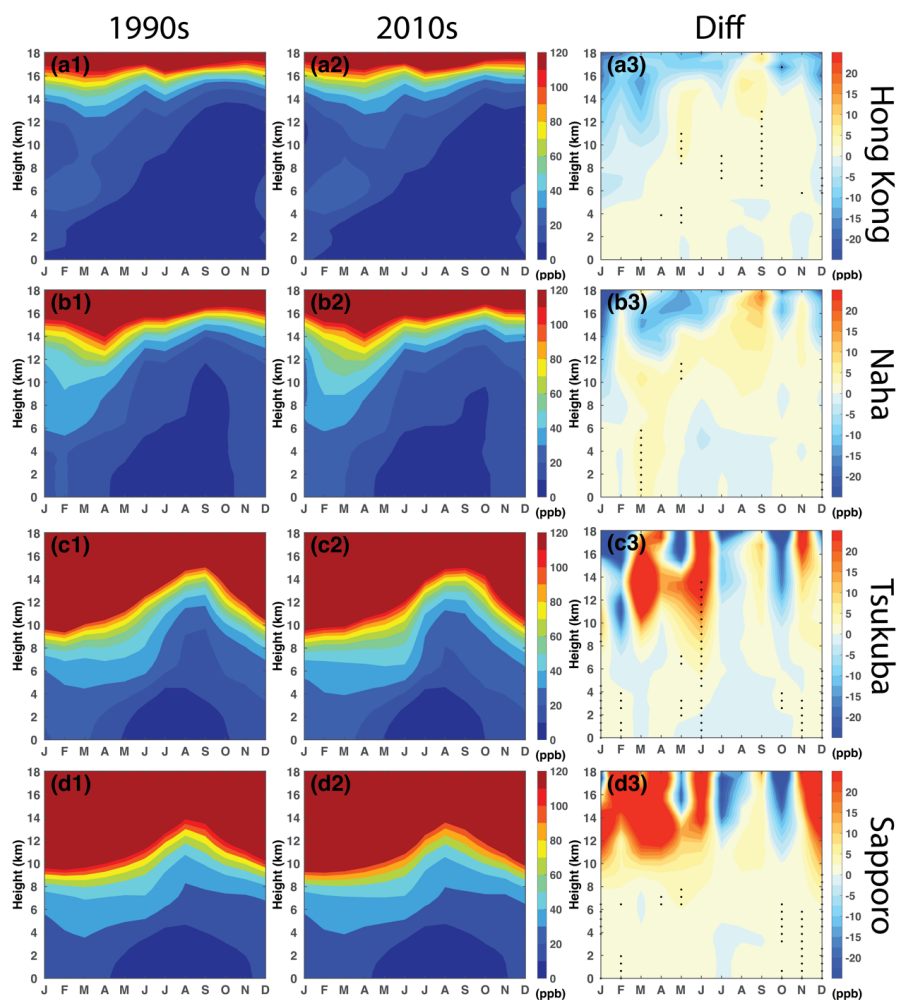
399 To gain deeper insights into the factors contributing to tropospheric O₃, we analyze the EMAC-simulated total O₃
400 in the troposphere, origin of O₃ from the stratosphere (i.e., stratospheric intrusion, O₃S), and origin of O₃ from the
401 troposphere (i.e., photochemical production in the troposphere, O₃T) at the four sites, along with their latitudinal
402 variations (Figures 9 and 10). The layer with the large mixing ratio of O₃S extending from the lower stratosphere
403 to the troposphere occurs in early spring in the southern site (i.e., Hong Kong). Conversely, similar occurrences
404 are observed to shift to early summer in the northern site (i.e., Sapporo) (Figure 9). The seasonal buildup of mid-
405 latitude total O₃ typically unfolds from winter through late spring, followed by a decline in summer (Fioletov and
406 Shepherd, 2003). Furthermore, together with dynamical processes such as tropopause folding in the vicinity of the
407 subtropical jet (Baray et al., 2000), stratospheric O₃ is transported downward into the troposphere. Over the past
408 30 years, the two sites within the subtropics (Tsukuba at 36°N and Sapporo at 43°N) exhibit larger O₃S increases
409 in the lower stratosphere and upper troposphere compared to the other two sites situated in the near-tropical region
410 (Hong Kong at 22°N and Naha at 26°N).

411

412 The O₃T shows seasonal maxima during the warm seasons (from March to October) throughout the troposphere
413 in Hong Kong, while mainly occurring in the middle to upper troposphere among three Japan sites (Figure 10). In
414 the lower troposphere at Hong Kong, the O₃T contributes more than O₃S (60-80 ppb vs. 10-20 ppb) in the separated
415 O₃ hotspots around 2-4km during spring. In the tropical regions, air rises in the Hadley cell from the surface to the
416 upper troposphere, and further ascent into the stratosphere where it is transported to the mid-latitudes by the
417 Brewer-Dobson Circulation (Brewer, 1949; A. Stohl et al., 2003). In this way, the tropospheric origin O₃ could be
418 further transported to the middle-upper troposphere of middle-latitude regions.

419

420 Several factors influence O₃ mixing ratios over study regions, which could potentially be responsible for the local
421 maxima in O₃T: transport from near-surface tropospheric O₃ within the upward branch of the Hadley cell into the
422 upper troposphere; horizontal transport from upstream polluted regions, e.g., mainland China in this study;
423 biomass burning related transport; enhanced mixture by active convection and lightning events; local photochemical
424 O₃ production. O₃T has shown significant enhancements among the four sites over the past several decades.
425 However, the primary contributors to the high O₃T concentrations and their enhancement vary with locations and
426 layers, which require further investigation.



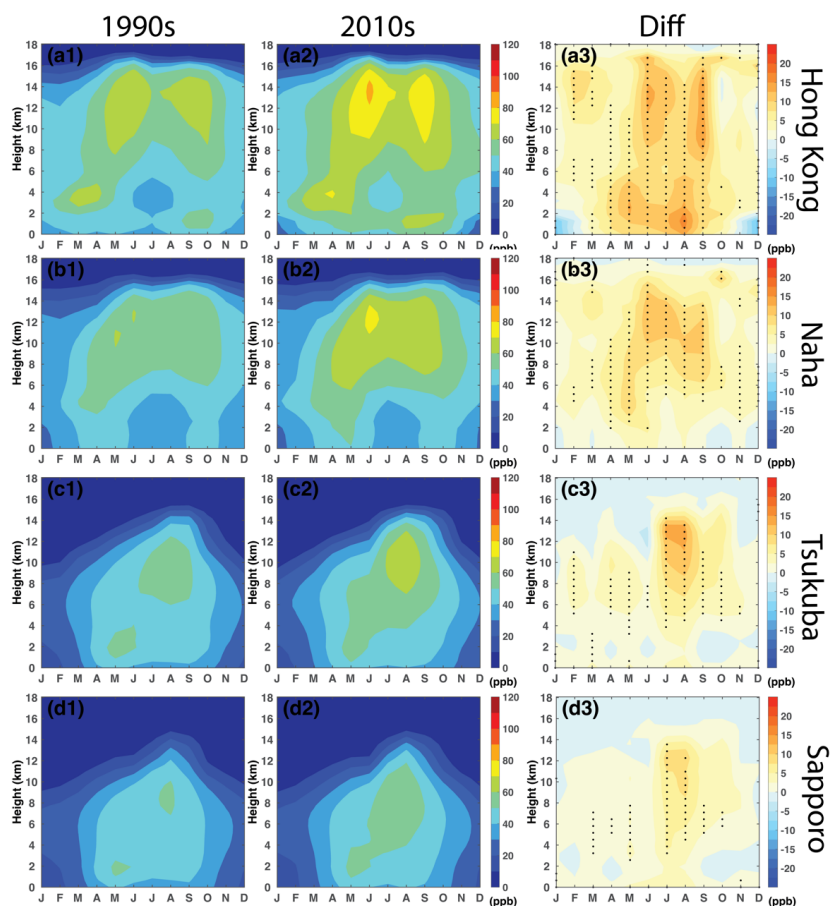
427

428

429

430

Figure 9. A comparison of the EMAC-simulated monthly mean temporal and spatial distributions of O₃S in the 1990s and 2010s, and the difference between 2010s and 1990s at the four observation sites: Hong Kong, Naha, Tsukuba, and Sapporo. Dots represent the layer with statistically significant changes according to a paired two-sided t-test ($p < 0.05$).



431

432 Figure 10. Similar to Figure 9 but for the component of tropospheric O₃ (O₃T).

433

434 **3.2.3 Quantification of stratospheric intrusion vs. tropospheric production using EMAC**

435 Utilizing the reasonably realistic simulations of tropospheric O₃ and their variations by the EMAC model, we can
 436 now quantify the respective contributions of O₃S and O₃T to the changes in tropospheric O₃ between the 2010s
 437 and 1990s, as presented in Table 3. Overall, the increase of O₃T (up to 11.09 ppb) dominates the O₃ increase
 438 throughout the troposphere at all the sites during summer. Particularly for the near-tropical sites, Hong Kong and
 439 Naha, the increase of O₃T contributes more than the O₃S changes with percentage contributions greatly much more
 440 than 60%, even offsetting the decrease in O₃S during winter and spring. Conversely, for the subtropical sites,
 441 Tsukuba and Sapporo, O₃S emerges as the primary driver for changes in the middle-upper tropospheric O₃ during
 442 winter and spring. The contribution of O₃S to observed O₃ increases by up to 96% and 40% in the middle-upper
 443 troposphere during winter and summer.

444

445

446

447

448



449

450 **Table 3. Contribution from O₃S and O₃T to changes of tropospheric O₃ between the 2010s and 1990s at the upper,**
 451 **middle, and lower troposphere (UT, MT, and LT) in different seasons. The percentage contributions of O₃S and O₃T to**
 452 **O₃ changes are listed in the parentheses.**

Station		O ₃ S changes (ppb)				O ₃ T changes (ppb)			
		MAM	JJA	SON	DJF	MAM	JJA	SON	DJF
Hong Kong	UT	-2.03 (-57%)	1.44 (11%)	1.41 (20%)	-3.44 (860%)	5.58 (157%)	11.09 (89%)	5.69 (80%)	3.04 (-760%)
	MT	1.30 (20%)	0.96 (10%)	1.23 (16%)	-2.84 (-888%)	5.06 (80%)	8.27 (90%)	6.27 (84%)	3.16 (988%)
	LT	0.88 (9%)	0.10 (1%)	-0.13 (-2%)	1.24 (59%)	8.73 (91%)	11.37 (99%)	6.41 (102%)	0.86 (41%)
Naha	UT	1.05 (18%)	3.81(26%)	2.98 (38%)	-1.87 (-143%)	4.90 (82%)	10.95 (74%)	4.78 (62%)	3.18 (243%)
	MT	2.32 (27%)	0.08 (1%)	1.10 (16%)	-1.03 (-47%)	6.19 (73%)	6.22 (99%)	5.64 (84%)	3.22 (147%)
	LT	2.35 (40%)	-0.19 (-6%)	0.07 (4%)	0.73 (43%)	3.51 (60%)	3.51 (106%)	1.68 (96%)	0.98 (57%)
Tsukuba	UT	7.33 (69%)	4.23 (40%)	2.19 (34%)	-4.59 (221%)	3.32 (31%)	7.22 (60%)	4.15 (66%)	2.51 (-121%)
	MT	1.50 (33%)	2.10 (28%)	1.39 (27%)	0.51 (19%)	3.04 (67%)	5.29 (72%)	3.79 (73%)	2.23 (81%)
	LT	1.27 (51%)	0.44 (20%)	0.94 (392%)	0.90 (92%)	1.22 (49%)	1.74 (80%)	-0.70 (-292%)	0.08 (8%)
Sapporo	UT	6.85 (79%)	3.19 (37%)	2.00 (39%)	4.65 (96%)	1.82 (21%)	5.40 (63%)	3.11 (61%)	0.17 (4%)
	MT	1.60 (42%)	1.59 (28%)	1.31 (34%)	1.62 (71%)	2.20 (58%)	4.14 (72%)	2.57 (66%)	0.65 (29%)
	LT	1.19 (50%)	0.35 (13%)	0.71 (263%)	0.69 (115%)	1.18 (50%)	2.45 (87%)	-0.45 (-163%)	-0.09 (-15%)

453

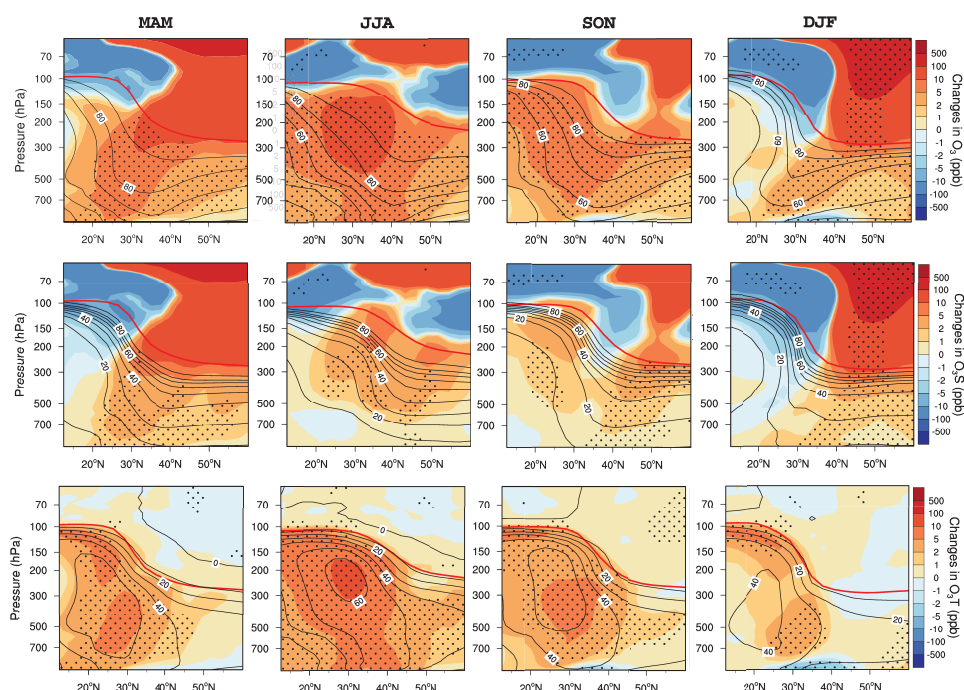
454 To get a more complete picture of how tropospheric O₃ changes along the Northwest Pacific regions, the zonal
 455 mean of tropospheric O₃, O₃S, and O₃T changes are compared in Figure 11. The climatological distribution of
 456 vertical tropospheric O₃ with latitude is determined by O₃S in the subtropics and O₃T in the tropics.

457

458 Tropospheric O₃ shows statistically significant positive changes from 10°N to 60°N in summer, with the maximum
 459 in the middle to upper troposphere around 30°N. Similarly, O₃T demonstrates a similar pattern of changes as
 460 tropospheric O₃ in summer, indicating that tropospheric photochemical O₃ production is the primary driver of the
 461 summertime tropospheric O₃ enhancement. Strengthened downward transport of stratospheric O₃ primarily affects
 462 the upper troposphere in the subtropics during summer.

463

464 Conversely, during winter and spring, the O₃S significantly contributes to the enhancement of tropospheric O₃ in
 465 the subtropics. Positive changes in O₃T are observed south of 40°N, partly offsetting the decrease in O₃S in the
 466 upper troposphere.



467
 468 **Figure 11. Latitude-pressure cross sections of mixing ratio difference of O_3 , O_3S , and O_3T (ppb) between the 2010s and**
 469 **1990s along the Northwest Pacific region (zonal mean over 110°N to 150°N) in four seasons. Black lines indicate the**
 470 **climatological distribution. Red solid lines denote the tropopause height. Dots represent the layer with statistically**
 471 **significant changes according to a paired two-sided t-test ($p < 0.05$).**

472

473 **4. Discussion and Conclusion**

474 In this study, thirty years of ozonesonde observational data at four ozonesonde sites (Hong Kong, Naha, Tsukuba,
 475 and Sapporo) are presented together with simulation results of the chemistry-climate model EMAC to characterize
 476 the temporal and spatial variation patterns and the long-term changes of tropospheric O_3 along the Northwest
 477 Pacific region.

478

479 The analysis of the seasonality in O_3 shows a seasonal maximum throughout the troposphere, occurring in late
 480 spring at the tropical site Hong Kong and shifting to early summer at the mid-latitude sites like Sapporo.
 481 Additionally, for Hong Kong and Naha, the lower tropospheric O_3 exhibits a seasonal minimum. As for long-term
 482 changes, tropospheric O_3 generally increases at all four sites. Naha and Tsukuba, show larger positive trends of
 483 O_3 up to 0.82 ppb a^{-1} , particularly in the upper and middle troposphere. The aggregation analysis between different
 484 decades indicates that the seasonal maximum in the troposphere becomes more pronounced and deeper over time.

485

486 Based on EMAC simulations, the summer and autumn enhancement of O_3 in the middle-upper troposphere is
 487 mostly attributable to tropospheric ozone source linked to increasing pollution emissions, with percentage
 488 contributions more than 60%. On the other hand, ozone originating from the stratosphere dominates the large



489 portion of middle-upper tropospheric O₃ enhancement by up to 96% and 40% in the mid-latitude during winter
490 and spring. The climatological maximum observed in the seasonality of ozone throughout the troposphere is
491 associated with both stratosphere-troposphere exchange north of 30°N and photochemical O₃ production in the
492 troposphere in spring. These findings corroborate the features discussed by Oltmans et al. (2004), confirming them
493 with a longer observational dataset based on the tagged ozone tracers in the EMAC model. Our results further
494 confirm the offsetting effect of O₃T increase to the decrease in O₃S in the tropical troposphere during winter and
495 spring.

496

497 While the magnitude of O₃ trends is well simulated with the EMAC model in most atmospheric layers,
498 uncertainties persist in the mean values due to various factors. These include large dynamical variability
499 perturbing stratosphere-to-troposphere O₃ transport, the influence of O₃-depleting substances, uncertainties of
500 long-term changes in emissions, insufficient treatment of chemical processes, or inaccurate transport due to
501 excessive numerical diffusion in the tropopause region, etc. Additionally, uncertainties may arise from
502 interpolating the relatively coarse horizontal and vertical resolution of the global model data to the locations of the
503 observational sites. Nevertheless, the presented results indicate a satisfactory level of agreement between the
504 model results and the observations, allowing further disentangling of O₃T versus O₃S contributions.

505

506 The dynamical and chemical drivers for such long-term tropospheric changes deserve further analysis in the future.
507 Here, we propose some mechanisms based on related research that could potentially contribute to observational
508 tropospheric O₃ enhancements in East Asia. Regional transport is one important contributor to tropospheric O₃
509 enhancement. Compared with the other two Japanese sites, Naha, to the east of China, is susceptible to regional
510 transport of air pollution from China. The prevailing westerly winds bring O₃-enriched air from eastern China to
511 Naha, resulting in a substantial increase of O₃ from the middle to upper troposphere. Internal dynamical
512 variabilities such as the warm phase of El Niño–Southern Oscillation (ENSO) and the easterly phase of the Quasi-
513 Biennial Oscillation (QBO) are known to be closely tied to enhanced STT of O₃ (Neu et al 2014, Zeng and Pyle,
514 2005). The ENSO/QBO-related changes can influence jet stream variations, leading to the formation of tropopause
515 folds through Rossby wave breaking (Albers et al 2018). Increased frequency and the northward shift of tropopause
516 folding events are observed in the East Asia region (Figure S3), attributed to an increase in the zonal wind and
517 poleward-upward shift of the STJ driven by global warming–induced increases in greenhouse gasses (Akritidis et
518 al 2019, Manney and Hegglin, 2018). With increasing greenhouse gasses, the Brewer-Dobson circulation tends to
519 strengthen due to larger zonal-mean temperature gradients and increased wave drag in the extratropical
520 stratosphere (Shepherd and McLandress, 2011; Neu et al 2014). This results in an increased O₃ reservoir over the
521 subtropical LMS, facilitating downward transport to the troposphere under the influence of the Pacific jet
522 (Hegglin and Shepherd, 2009; Albers et al 2018).

523

524 **Data Availability Statement:** The ozone-sounding dataset used for observational analysis in the study is publicly
525 available at the World Ozone and Ultraviolet Radiation Data Centre via
526 <https://woudc.org/data/explore.php?lang=en> (last access: 25 Feb 2024).

527

528 **Supplement:** Supplementary.pdf



529

530

531 **Author Contributions:** XM carried out all the observational and model simulation data analyses, led the
532 interpretation of the results, and prepared the manuscript with contributions from all the co-authors. JH, MH, PJ,
533 and TZ contributed to the interpretation of the results and provided extensive comments on the manuscript. PJ
534 conducted the EMAC simulations.

535

536 **Competing interests:** At least one of the (co-)authors is a member of the editorial board of Atmospheric Chemistry
537 and Physics.

538

539 **Acknowledgment:** This research has been supported by the National Key Research and Development Program
540 of China (2022YFC3701204), the National Natural Science Foundation of China (42275196, 42105164), and the
541 Applied Basic Research Foundation (2022A1515011078). The EMAC simulations have been performed at the
542 German Climate Computing Centre (DKRZ) through support from the Bundesministerium für Bildung und
543 Forschung (BMBF). DKRZ and its scientific steering committee are gratefully acknowledged for providing the
544 HPC and data archiving resources for this consortial project ESCiMo (Earth System Chemistry integrated
545 Modelling). We especially thank the Michael Sprenger from ETH Zurich for providing the tropopause folding
546 frequency dataset.

547

548 **References**

549 Akritidis, D., Pozzer, A., and Zanis, P.: On the impact of future climate change on tropopause folds and
550 tropospheric ozone, *Atmos. Chem. Phys.*, 19, 14387-14401, <https://doi.org/10.5194/acp-19-14387-2019>, 2019.

551 Albers, J. R., Perlwitz, J., Butler, A. H., Birner, T., Kiladis, G. N., Lawrence, Z. D., Manney, G. L., Langford, A.
552 O., and Dias, J.: Mechanisms governing interannual variability of stratosphere-to-troposphere ozone transport, *J.*
553 *Geophys. Res.*, 123, 234-260, <https://doi.org/10.1002/2017JD026890>, 2018.

554 Bak, J., Baek, K. H., Kim, J. H., Liu, X., Kim, J., and Chance, K.: Cross-evaluation of GEMS tropospheric ozone
555 retrieval performance using OMI data and the use of an ozonesonde dataset over East Asia for validation, *Atmos.*
556 *Meas. Tech.*, 12, 5201-5215, <https://doi.org/10.5194/amt-12-5201-2019>, 2019.

557 Baray, J.-L., Daniel, V., Ancellet, G., and Legras, B.: Planetary-scale tropopause folds in the southern subtropics,
558 *Geophys. Res. Lett.*, 27, 353-356, <https://doi.org/10.1029/1999GL010788>, 2000.

559 Brewer, A. W.: Evidence for a world circulation provided by the measurements of helium and water vapour
560 distribution in the stratosphere, *Q. J. Roy. Meteor. Soc.*, 75, 351-363, <https://doi.org/10.1002/qj.49707532603>,
561 1949.

562 Chang, K.-L., Petropavlovskikh, I., Cooper, O. R., Schultz, M. G., and Wang, T.: Regional trend analysis of surface
563 ozone observations from monitoring networks in eastern North America, Europe and East Asia, *Elem. Sci. Anth.*,
564 5, <https://doi.org/10.1525/elementa.243>, 2017.

565 Collins, J. W.: Effect of stratosphere-troposphere exchange on the future tropospheric ozone trend, *J. Geophys.*
566 *Res.*, 108, <https://doi.org/10.1029/2002JD002617>, 2003.

567 Cooper, O. R., Parrish, D. D., Ziemke, J., Balashov, N. V., Cupeiro, M., Galbally, I. E., Gilge, S., Horowitz, L.,
568 Jensen, N. R., Lamarque, J.-F., Naik, V., Oltmans, S. J., Schwab, J., Shindell, D. T., Thompson, A. M., Thouret,
569 V., Wang, Y., and Zbinden, R. M.: Global distribution and trends of tropospheric ozone: An observation-based
570 review, *Elem. Sci. Anth.*, 2, <https://doi.org/10.12952/journal.elementa.000029>, 2014.

571 Ding, A. J., and Wang, T.: Influence of stratosphere-to-troposphere exchange on the seasonal cycle of surface
572 ozone at Mount Waliguan in western China, *Geophys. Res. Lett.*, 33, L03803,
573 <https://doi.org/10.1029/2005GL024760>, 2006.

574 Ding, A. J., Wang, T., and Fu, C. B.: Transport characteristics and origins of carbon monoxide and ozone in Hong
575 Kong, South China, *J. Geophys. Res.*, 118, 9475-9488, <https://doi.org/10.1002/jgrd.50714>, 2013.



- 576 Duncan, B. N., Lamsal, L. N., Thompson, A. M., Yoshida, Y., Lu, Z., Streets, D. G., Hurwitz, M. M., and Pickering,
577 K. E.: A space-based, high-resolution view of notable changes in urban NO_x pollution around the world (2005–
578 2014), *J. Geophys. Res.*, 121, 976–996, <https://doi.org/10.1002/2015JD024121>, 2016.
- 579 Fioletov, V. E., and Shepherd, T. G.: Seasonal persistence of midlatitude total ozone anomalies, *Geophys. Res.*
580 *Letts.*, 30, <https://doi.org/10.1029/2002GL016739>, 2003.
- 581 Granier, C., Bessagnet, B., Bond, T., D’Angiola, A., Denier van der Gon, H., Frost, G. J., Heil, A., Kaiser, J. W.,
582 Kinne, S., Klimont, Z., Kloster, S., Lamarque, J.-F., Liousse, C., Masui, T., Meleux, F., Mieville, A., Ohara, T.,
583 Raut, J.-C., Riahi, K., Schultz, M. G., Smith, S. J., Thompson, A., van Aardenne, J., van der Werf, G. R., and van
584 Vuuren, D. P.: Evolution of anthropogenic and biomass burning emissions of air pollutants at global and regional
585 scales during the 1980–2010 period, *Clim. Change.*, 109, 163, <https://doi.org/10.1007/s10584-011-0154-1>, 2011.
- 586 Griffiths, P. T., Keeble, J., Shin, Y. M., Abraham, N. L., Archibald, A. T., and Pyle, J. A.: On the Changing Role
587 of the Stratosphere on the Tropospheric Ozone Budget: 1979–2010, *Geophys. Res. Letts.*, 47, e2019GL086901,
588 <https://doi.org/10.1029/2019GL086901>, 2020.
- 589 Hegglin, M. I., and Shepherd, T. G.: Large climate-induced changes in ultraviolet index and stratosphere-to-
590 troposphere ozone flux, *Nat. Geosci.*, 2, 687–691, <https://doi.org/10.1038/ngeo604>, 2009.
- 591 Hersbach, H., Bell, B., Berrisford, P., Hirahara, S., Horányi, A., Muñoz-Sabater, J., Nicolas, J., Peubey, C., Radu,
592 R., Schepers, D., Simmons, A., Soci, C., Abdalla, S., Abellan, X., Balsamo, G., Bechtold, P., Biavati, G., Bidlot,
593 J., Bonavita, M., De Chiara, G., Dahlgren, P., Dee, D., Diamantakis, M., Dragani, R., Flemming, J., Forbes, R.,
594 Fuentes, M., Geer, A., Haimberger, L., Healy, S., Hogan, R. J., Hölm, E., Janisková, M., Keeley, S., Laloyaux, P.,
595 Lopez, P., Lupu, C., Radnoti, G., de Rosnay, P., Rozum, I., Vamborg, F., Villaume, S., and Thépaut, J.-N.: The
596 ERA5 global reanalysis, *Q. J. R. Meteorol. Soc.*, 146, 1999–2049, <https://doi.org/10.1002/qj.3803>, 2020.
- 597 Holton, J. R., Haynes, P. H., McIntyre, M. E., Douglass, A. R., Rood, R. B., and Pfister, L.: Stratosphere-
598 troposphere exchange, *Rev. Geophys.*, 33, 403–439, <https://doi.org/10.1029/95RG02097>, 1995.
- 599 Huang, J. P., Fung, J. C., Lau, A. K., and Qin, Y.: Numerical simulation and process analysis of typhoon-related
600 ozone episodes in Hong Kong, *J. Geophys. Res.*, 110, <https://doi.org/10.1029/2004JD004914>, 2005.
- 601 Jöckel, P., Tost, H., Pozzer, A., Brühl, C., Buchholz, J., Ganzeveld, L., Hoor, P., Kerkweg, A., Lawrence, M. G.,
602 Sander, R., Steil, B., Stiller, G., Tanarhte, M., Taraborrelli, D., van Aardenne, J., and Lelieveld, J.: The atmospheric
603 chemistry general circulation model ECHAM5/MESSy1: consistent simulation of ozone from the surface to the
604 mesosphere, *Atmos. Chem. Phys.*, 6, 5067–5104, <https://doi.org/10.5194/acp-6-5067-2006>, 2006.
- 605 Jöckel, P., Tost, H., Pozzer, A., Kunze, M., Kirner, O., Brenninkmeijer, C. A. M., Brinkop, S., Cai, D. S., Dyroff,
606 C., Eckstein, J., Frank, F., Garny, H., Gottschaldt, K. D., Graf, P., Grewe, V., Kerkweg, A., Kern, B., Matthes, S.,
607 Mertens, M., Meul, S., Neumaier, M., Nützel, M., Oberländer-Hayn, S., Ruhnke, R., Runde, T., Sander, R.,
608 Scharffe, D., and Zahn, A.: Earth System Chemistry integrated Modelling (ESCiMo) with the Modular Earth
609 Submodel System (MESSy) version 2.51, *Geosci. Model Dev.*, 9, 1153–1200, <https://doi.org/10.5194/gmd-9-1153-2016>, 2016.
- 611 Jöckel, P.: CCMi-2022: refD1 data produced by the EMAC-CCMI2 model at MESSy-Consortium, in, edited by:
612 Analysis, E. E. C. f. E. D., 2023.
- 613 Johnson, B. J., Oltmans, S. J., Vömel, H., Smit, H. G. J., Deshler, T., and Kröger, C.: Electrochemical
614 concentration cell (ECC) ozonesonde pump efficiency measurements and tests on the sensitivity to ozone of
615 buffered and unbuffered ECC sensor cathode solutions, *J. Geophys. Res.*, 107, ACH 8-1-ACH 8-18,
616 <https://doi.org/10.1029/2001JD000557>, 2002.
- 617 Kerkweg, A., Sander, R., Tost, H., and Jöckel, P.: Technical note: Implementation of prescribed (OFFLEM),
618 calculated (ONLEM), and pseudo-emissions (TNUDGE) of chemical species in the Modular Earth Submodel
619 System (MESSy), *Atmos. Chem. Phys.*, 6, 3603–3609, <https://doi.org/10.5194/acp-6-3603-2006>, 2006.
- 620 Krotkov, N. A., McLinden, C. A., Li, C., Lamsal, L. N., Celarier, E. A., Marchenko, S. V., Swartz, W. H., Bucsela,
621 E. J., Joiner, J., Duncan, B. N., Boersma, K. F., Veefkind, J. P., Levelt, P. F., Fioletov, V. E., Dickerson, R. R.,
622 He, H., Lu, Z., and Streets, D. G.: Aura OMI observations of regional SO₂ and NO₂ pollution changes from 2005
623 to 2015, *Atmos. Chem. Phys.*, 16, 4605–4629, <https://doi.org/10.5194/acp-16-4605-2016>, 2016.
- 624 Kunze, M., Godolt, M., Langematz, U., Grenfell, J. L., Hamann-Reinus, A., and Rauer, H.: Investigating the early
625 Earth faint young Sun problem with a general circulation model, *Planet. Space Sci.*, 98, 77–92,
626 <https://doi.org/10.1016/j.pss.2013.09.011>, 2014.
- 627 Li, K., Jacob, D. J., Liao, H., Shen, L., Zhang, Q., and Bates, K. H.: Anthropogenic drivers of 2013–2017 trends
628 in summer surface ozone in China, *P. Natl. Acad. Sci.*, 116, 422–427, <https://doi.org/10.1073/pnas.1812168116>
629 2019.



- 630 Liao, Z., Ling, Z., Gao, M., Sun, J., Zhao, W., Ma, P., Quan, J., and Fan, S.: Tropospheric Ozone Variability Over
631 Hong Kong Based on Recent 20 years (2000–2019) Ozonesonde Observation, *J. Geophys. Res.*, 126,
632 e2020JD033054, <https://doi.org/10.1029/2020JD033054>, 2021.
- 633 Lin, C., Leung, K. K., Alfred, L., Tsang, R. C., Tsui, W. B., Fung, J. C., Ng, E. K., Cheung, S., Tang, A. W., and
634 Ning, Z.: Effects of synoptic patterns on the vertical structure of ozone in Hong Kong using lidar measurement,
635 *Atmos. Environ.*, 257, 118490, <https://doi.org/10.1016/j.atmosenv.2021.118490>, 2021.
- 636 Liu, F., Zhang, Q., van der A, R. J., Zheng, B., Tong, D., Yan, L., Zheng, Y., and He, K.: Recent reduction in NOx
637 emissions over China: synthesis of satellite observations and emission inventories, *Environ. Res. Lett.*, 11, 114002,
638 <https://doi.org/10.1088/1748-9326/11/11/114002>, 2016.
- 639 Liu, H., Jacob, D. J., Chan, L. Y., Oltmans, S. J., Bey, I., Yantosca, R. M., Harris, J. M., Duncan, B. N., and Martin,
640 R. V.: Sources of tropospheric ozone along the Asian Pacific Rim: An analysis of ozonesonde observations, *J.*
641 *Geophys. Res.*, 107, ACH 3-1-ACH 3-19, <https://doi.org/10.1029/2001JD002005>, 2002.
- 642 Ma, Z., Xu, J., Quan, W., Zhang, Z., Lin, W., and Xu, X.: Significant increase of surface ozone at a rural site,
643 north of eastern China, *Atmos. Chem. Phys.*, 16, 3969-3977, <https://doi.org/10.5194/acp-16-3969-2016>, 2016.
- 644 Manney, G. L., and Hegglin, M. I.: Seasonal and regional variations of long-term changes in upper-tropospheric
645 jets from reanalyses, *J. Climate.*, 31, 423-448, <https://doi.org/10.1175/JCLI-D-17-0303.1>, 2018.
- 646 Meul, S., Langematz, U., Kröger, P., Oberländer-Hayn, S., and Jöckel, P.: Future changes in the stratosphere-to-
647 troposphere ozone mass flux and the contribution from climate change and ozone recovery, *Atmos. Chem. Phys.*,
648 18, 7721-7738, <https://doi.org/10.5194/acp-18-7721-2018>, 2018.
- 649 Miyazaki, K., Eskes, H., Sudo, K., Boersma, K. F., Bowman, K., and Kanaya, Y.: Decadal changes in global
650 surface NOx emissions from multi-constituent satellite data assimilation, *Atmos. Chem. Phys.*, 17, 807-837,
651 <https://doi.org/10.5194/acp-17-807-2017>, 2017.
- 652 Morgenstern, O., Hegglin, M. I., Rozanov, E., O'Connor, F. M., Abraham, N. L., Akiyoshi, H., Archibald, A. T.,
653 Bekki, S., Butchart, N., Chipperfield, M. P., Deushi, M., Dhomse, S. S., Garcia, R. R., Hardiman, S. C., Horowitz,
654 L. W., Jöckel, P., Josse, B., Kinnison, D., Lin, M., Mancini, E., Manyin, M. E., Marchand, M., Marécal, V., Michou,
655 M., Oman, L. D., Pitari, G., Plummer, D. A., Revell, L. E., Saint-Martin, D., Schofield, R., Stenke, A., Stone, K.,
656 Sudo, K., Tanaka, T. Y., Tilmes, S., Yamashita, Y., Yoshida, K., and Zeng, G.: Review of the global models used
657 within phase 1 of the Chemistry–Climate Model Initiative (CCMI), *Geosci. Model Dev.*, 10, 639-671,
658 <https://doi.org/10.5194/gmd-10-639-2017>, 2017.
- 659 Morris, G. A., Labow, G., Akimoto, H., Takigawa, M., Fujiwara, M., Hasebe, F., Hirokawa, J., and Koide, T.: On
660 the use of the correction factor with Japanese ozonesonde data, *Atmos. Chem. Phys.*, 13, 1243-1260,
661 <https://doi.org/10.5194/acp-13-1243-2013>, 2013.
- 662 Neu, J. L., Flury, T., Manney, G. L., Santee, M. L., Livesey, N. J., and Worden, J.: Tropospheric ozone variations
663 governed by changes in stratospheric circulation, *Nat. Geosci.*, 7, 340-344, <https://doi.org/10.1038/ngeo2138>,
664 2014.
- 665 Oltmans, S. J., Johnson, B. J., Harris, J. M., and Thompson, A. M.: Tropospheric ozone over the North Pacific
666 from ozonesonde observations, *J. Geophys. Res.*, <https://doi.org/10.1029/2003JD003466>, 2004.
- 667 Revell, L. E., Stenke, A., Tummon, F., Feinberg, A., Rozanov, E., Peter, T., Abraham, N. L., Akiyoshi, H.,
668 Archibald, A. T., Butchart, N., Deushi, M., Jöckel, P., Kinnison, D., Michou, M., Morgenstern, O., O'Connor, F.
669 M., Oman, L. D., Pitari, G., Plummer, D. A., Schofield, R.,
- 670 Stone, K., Tilmes, S., Visioni, D., Yamashita, Y., and Zeng, G.: Tropospheric ozone in CCMI models and Gaussian
671 process emulation to understand biases in the SOCOLv3 chemistry–climate model, *Atmos. Chem. Phys.*, 18,
672 16155-16172, <https://doi.org/10.5194/acp-18-16155-2018>, 2018.
- 673 Roelofs, G.-J., and Lelieveld, J.: Model study of the influence of cross-tropopause O3 transports on tropospheric
674 O3 levels, *Tellus. B.*, 49, 38-55, <https://doi.org/10.3402/tellusb.v49i1.15949>, 1997.
- 675 Sander, R., Baumgaertner, A., Gromov, S., Harder, H., Jöckel, P., Kerkweg, A., Kubistin, D., Regelin, E., Riede,
676 H., Sandu, A., Taraborrelli, D., Tost, H., and Xie, Z. Q.: The atmospheric chemistry box model CAABA/MECCA-
677 3.0, *Geosci. Model Dev.*, 4, 373-380, <https://doi.org/10.5194/gmd-4-373-2011>, 2011.
- 678 Sander, R., Jöckel, P., Kirner, O., Kunert, A. T., Landgraf, J., and Pozzer, A.: The photolysis module JVAL-14,
679 compatible with the MESSy standard, and the JVal PreProcessor (JVPP), *Geosci. Model Dev.*, 7, 2653-2662,
680 <https://doi.org/10.5194/gmd-7-2653-2014>, 2014.
- 681 Shepherd, T. G., and McLandress, C.: A Robust Mechanism for Strengthening of the Brewer–Dobson Circulation
682 in Response to Climate Change: Critical-Layer Control of Subtropical Wave Breaking, *J. Atmos. Sci.*, 68, 784-
683 797, <https://doi.org/10.1175/2010JAS3608.1>, 2011.



- 684 Škerlak, B., Sprenger, M., Pfahl, S., Tyrlis, E., and Wernli, H.: Tropopause folds in ERA-Interim: Global
685 climatology and relation to extreme weather events, *J. Geophys. Res.*, 120, 4860–4877,
686 <https://doi.org/10.1002/2014JD022787>, 2015.
- 687 SPARC CCMVal: SPARC Report on the Evaluation of Chemistry Climate Models, edited by: Eyring, V.,
688 Shepherd, T. G., and Waugh, D. W., SPARC Report No. 5, WCRP-132, WMO/TD-No. 1526, [http://www.sparc-](http://www.sparc-climate.org/publications/sparc-reports/)
689 [climate.org/publications/sparc-reports/](http://www.sparc-climate.org/publications/sparc-reports/), 2010
- 690 Sprenger, M., Maspoli, M. C., and Wernli, H.: Tropopause folds and cross-tropopause exchange. A global
691 investigation based upon ECMWF analyses for the time period March 2000 to February 2001, *J. Geophys. Res.*,
692 108, <https://doi.org/10.1029/2002JD002587>, 2003.
- 693 Stohl, A., P. Bonasoni, P. Cristofanelli, W. Collins, J. Feichter, A. Frank, C. Forster, E. Gerasopoulos, H. Gaggeler,
694 P. James, T. Kentarchos, H. Kromp-Kolb, B. Krüger, C. Land, J. Meloen, A. Papayannis, A. Priller, P. Seibert,
695 M. Sprenger, G. J. Roelofs, H. E. Scheel, C. Schnabel, P. Siegmund, L. Tobler, T. Trickl, H. Wernli, V. Wirth, P.
696 Zanis, and Zerefos, C.: Stratosphere-troposphere exchange: A review, and what we have learned from
697 STACCATO, *J. Geophys. Res.*, <https://doi.org/10.1029/2002JD002490>, 2003.
- 698 Su, T., Li, J., Li, C., Xiang, P., Lau, A. K.-H., Guo, J., Yang, D., and Miao, Y.: An intercomparison of long-term
699 planetary boundary layer heights retrieved from CALIPSO, ground-based lidar, and radiosonde measurements
700 over Hong Kong, *J. Geophys. Res.*, 122, 3929–3943, <https://doi.org/10.1002/2016JD025937>, 2017.
- 701 Sudo, K., Takahashi, M., and Akimoto, H.: Future changes in stratosphere-troposphere exchange and their impacts
702 on future tropospheric ozone simulations, *Geophys. Res. Lett.*, 30, 2256, <https://doi.org/10.1029/2003GL018526>,
703 2003.
- 704 Sun, L., Xue, L., Wang, T., Gao, J., Ding, A., Cooper, O. R., Lin, M., Xu, P., Wang, Z., Wang, X., Wen, L., Zhu,
705 Y., Chen, T., Yang, L., Wang, Y., Chen, J., and Wang, W.: Significant increase of summertime ozone at Mount
706 Tai in Central Eastern China, *Atmos. Chem. Phys.*, 16, 10637–10650, <https://doi.org/10.5194/acp-16-10637-2016>,
707 2016.
- 708 Tost, H., Jöckel, P., Kerkweg, A., Sander, R., and Lelieveld, J.: Technical note: A new comprehensive
709 SCAVenging submodel for global atmospheric chemistry modelling, *Atmos. Chem. Phys.*, 6, 565–574,
710 <https://doi.org/10.5194/acp-6-565-2006>, 2006.
- 711 Tost, H., Jöckel, P., and Lelieveld, J.: Lightning and convection parameterisations & uncertainties in global
712 modelling, *Atmos. Chem. Phys.*, 7, 4553–4568, <https://doi.org/10.5194/acp-7-4553-2007>, 2007.
- 713 Trickl, T., Bärtsch-Ritter, N., Eisele, H., Furger, M., Mücke, R., Sprenger, M., and Stohl, A.: High-ozone layers
714 in the middle and upper troposphere above Central Europe: potential import from the stratosphere along the
715 subtropical jet stream, *Atmos. Chem. Phys.*, 11, 9343–9366, <https://doi.org/10.5194/acp-11-9343-2011>, 2011.
- 716 van der A, R. J., Mijling, B., Ding, J., Koukouli, M. E., Liu, F., Li, Q., Mao, H., and Theys, N.: Cleaning up the
717 air: effectiveness of air quality policy for SO₂ and NO_x emissions in China, *Atmos. Chem. Phys.*, 17, 1775–1789,
718 <https://doi.org/10.5194/acp-17-1775-2017>, 2017.
- 719 Verstraeten, W. W., Neu, J. L., Williams, J. E., Bowman, K. W., Worden, J. R., and Boersma, K. F.: Rapid
720 increases in tropospheric ozone production and export from China, *Nat. Geosci.*, 8, 690–695,
721 <https://doi.org/10.1038/NGEO2493>, 2015.
- 722 Wang, T., Xue, L., Brimblecombe, P., Lam, Y. F., Li, L., and Zhang, L.: Ozone pollution in China: A review of
723 concentrations, meteorological influences, chemical precursors, and effects, *Sci. Total Environ.*, 575, 1582–1596,
724 <https://doi.org/10.1016/j.scitotenv.2016.10.081>, 2017.
- 725 Williams, R. S., Hegglin, M. I., Kerridge, B. J., Jöckel, P., Latter, B. G., and Plummer, D. A.: Characterising the
726 seasonal and geographical variability in tropospheric ozone, stratospheric influence and recent changes, *Atmos.*
727 *Chem. Phys.*, 19, 3589–3620, <https://doi.org/10.5194/acp-19-3589-2019>, 2019.
- 728 Witte, J. C., Thompson, A. M., Smit, H. G. J., Vömel, H., Posny, F., and Stübi, R.: First Reprocessing of Southern
729 Hemisphere Additional OZonesondes Profile Records: 3. Uncertainty in Ozone Profile and Total Column, *J.*
730 *Geophys. Res.*, 123, 3243–3268, <https://doi.org/10.1002/2017JD027791>, 2018.
- 731 World Meteorological Organization: Meteorology: A three dimensional science, 6, 134–138, 1957.
- 732 Xu, W., Lin, W., Xu, X., Tang, J., Huang, J., Wu, H., and Zhang, X.: Long-term trends of surface ozone and its
733 influencing factors at the Mt Waliguan GAW station, China – Part 1: Overall trends and characteristics, *Atmos.*
734 *Chem. Phys.*, 16, 6191–6205, <https://doi.org/10.5194/acp-16-6191-2016>, 2016.
- 735 Young, P. J., Naik, V., Fiore, A. M., Gaudel, A., Guo, J., Lin, M. Y., Neu, J. L., Parrish, D. D., Rieder, H. E.,
736 Schnell, J. L., Tilmes, S., Wild, O., Zhang, L., Ziemke, J., Brandt, J., Delcloo, A., Doherty, R. M., Geels, C.,
737 Hegglin, M. I., Hu, L., Im, U., Kumar, R., Luhar, A., Murray, L., Plummer, D., Rodriguez, J., Saiz-Lopez, A.,



- 738 Schultz, M. G., Woodhouse, M. T., and Zeng, G.: Tropospheric Ozone Assessment Report: Assessment of global-
739 scale model performance for global and regional ozone distributions, variability, and trends, *Elem. Sci. Anth.*, 6,
740 <https://doi.org/10.1525/elementa.265>, 2018.
- 741 Zeng, G., and Pyle, J. A.: Influence of El Niño Southern Oscillation on stratosphere/troposphere exchange and the
742 global tropospheric ozone budget, *Geophys. Res. Lett.*, 32, <https://doi.org/10.1029/2004GL021353>, 2005.
- 743 Zhang, Y., Liu, H., Crawford, J. H., Considine, D. B., Chan, C., Oltmans, S. J., and Thouret, V.: Distribution,
744 variability and sources of tropospheric ozone over south China in spring: Intensive ozonesonde measurements at
745 five locations and modeling analysis, *J. Geophys. Res.*, 117, <https://doi.org/10.1029/2012JD017498>, 2012.
- 746 Zhang, Y., Cooper, O. R., Gaudel, A., Thompson, A. M., Nédélec, P., Ogino, S.-Y., and West, J. J.: Tropospheric
747 ozone change from 1980 to 2010 dominated by equatorward redistribution of emissions, *Nat. Geosci.*, 9, 875-879,
748 <https://doi.org/10.1038/ngeo2827>, 2016.
- 749 Zhao, K., Huang, J., Wu, Y., Yuan, Z., Wang, Y., Li, Y., Ma, X., Liu, X., Ma, W., Wang, Y., and Zhang, X.:
750 Impact of stratospheric intrusions on ozone enhancement in the lower troposphere and implication to air quality
751 in Hong Kong and other South China regions, *J. Geophys. Res.*, 126, e2020JD033955,
752 <https://doi.org/10.1029/2020JD033955>, 2021.
- 753 Zhou, D., Ding, A., Mao, H., Fu, C., Wang, T., Chan, L. Y., Ding, K., Zhang, Y., Liu, J., Lu, A., and Hao, N.:
754 Impacts of the East Asian monsoon on lower tropospheric ozone over coastal South China, *Environ. Res. Lett.*, 8,
755 044011, <https://doi.org/10.1088/1748-9326/8/4/044011>, 2013.
- 756